

Supplementary Materials for

Noninvasive neuroimaging enhances continuous neural tracking for robotic device control

¹B. J. Edelman, ²†J. Meng, ²†D. Suma, ¹C. Zurn, ³E. Nagarajan, ¹B. S. Baxter, ¹C. C. Cline, ^{1,2}*B. He

¹Department of Biomedical Engineering, University of Minnesota, Minneapolis, MN 55455, USA

²Department of Biomedical Engineering, Carnegie Mellon University, Pittsburgh, PA 15213, USA

³Department of Neuroscience, University of Minnesota, Minneapolis, MN 55455, USA

Correspondence to: bhe1@andrew.cmu.edu

This PDF file includes:

Figs. S1 to S9

Tables S1 to S2

Captions for Videos S1 to S7

Other Supplementary Materials for this manuscript include the following:

Videos S1 to S7

Fig. S1.

Supplementary Figure 1 displays example trials of neural virtual cursor tracking trajectories for the original continuous pursuit task. Fig. S1c illustrates the trajectory unwrapping method. First, the target positions were subtracted from the cursor positions (both between 0 and 1) to obtain an error time series. A -1 was added to cursor position indices when the error was greater than 0.5, and a +1 was added to those when the error was less than -0.5. These cases represent instances where the cursor deviated slightly from the target near an edge and wrapped to the other side of the workspace (red circles). Such behavior and dramatic changes in relative position can significantly penalize the correlation calculation, even though tracking performance is still quite good. The unwrapped trajectory therefore corrected for these cases by reconstructing accurate relative trajectories (red arrows).

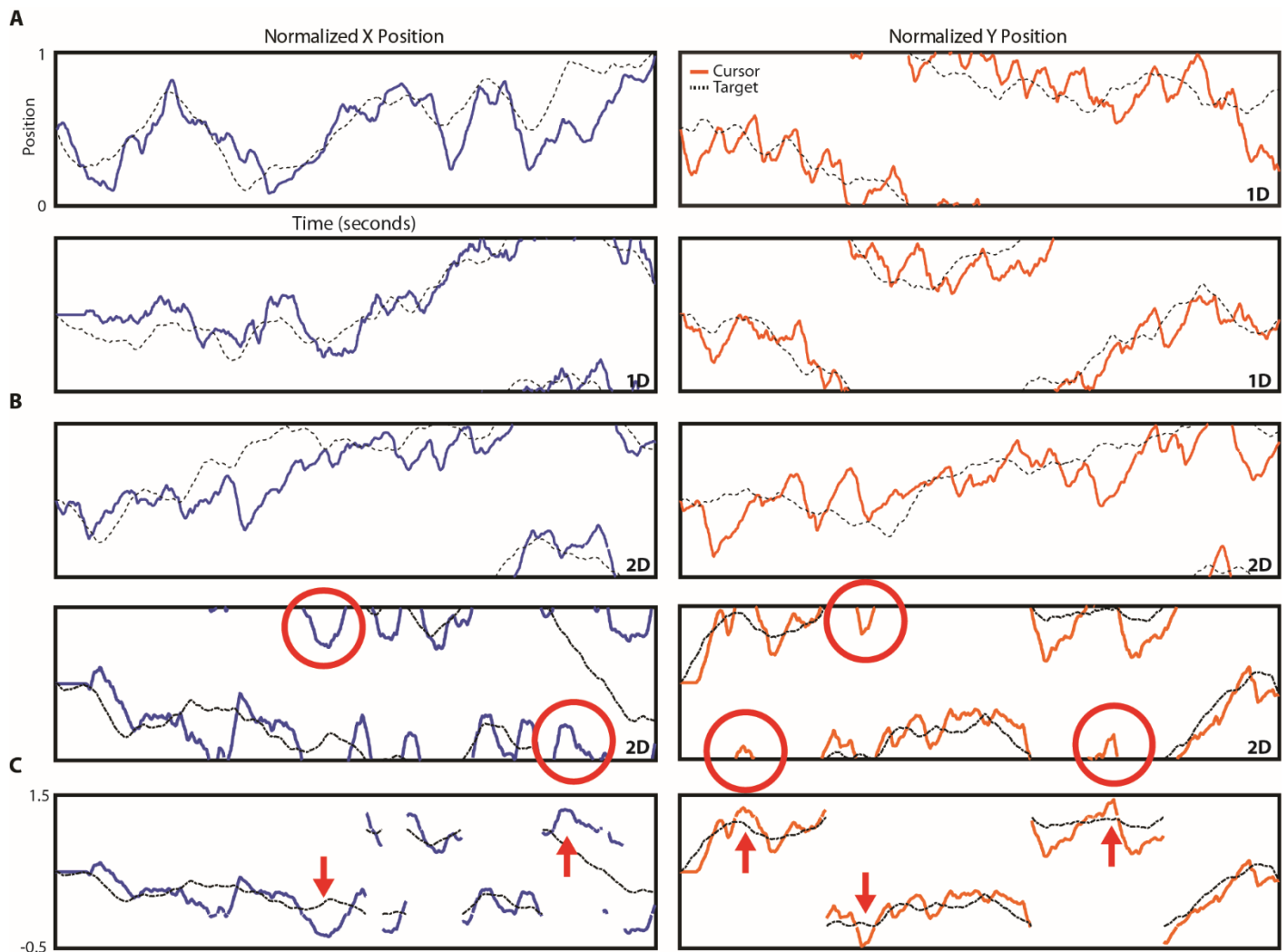


Figure S1. Example Continuous Pursuit Trajectories. (A) Normalized cursor and target trajectories for 1D horizontal (left) and 1D vertical (right) trials. (B) Cursor and target trajectories for 2D trials. Red circles in the bottom row highlight instances of horizontal (left) and vertical (right) cursor edge wraps. (C) Unwrapped 2D trajectories for the trial in the bottom row of (B). Red arrows highlight where the unwrapping procedure mitigates tracking biases resulting from the edge wrapping procedure.

Fig. S2.

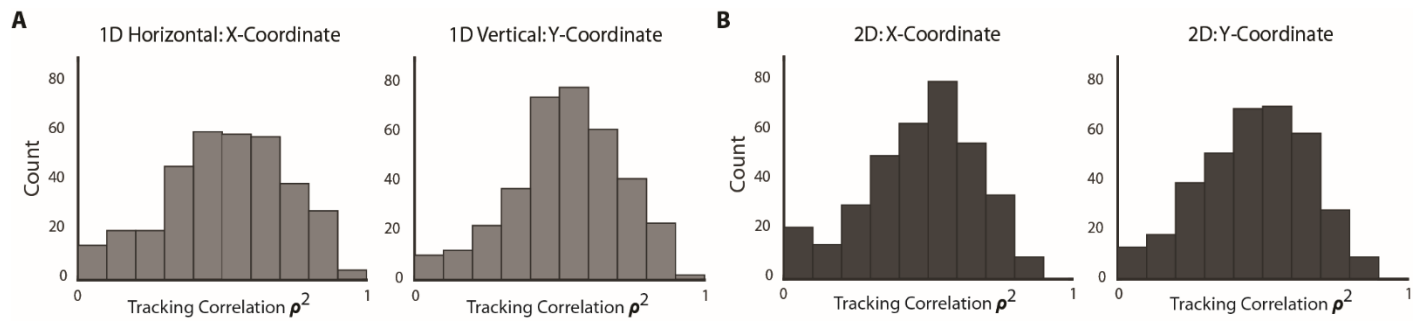


Figure S2. Squared Tracking Correlation Histograms. (A) Histograms of **squared** tracking correlation values (ρ^2) for the X-coordinate (left) and Y-coordinate (right) during 1D horizontal and 1D vertical trials, respectively. (B) Histograms of **squared** tracking correlation values (ρ^2) for the X-coordinate (left) and Y-coordinate (right) during 2D trials. Histograms are composed of ~ 350 trials each.

Fig. S3.

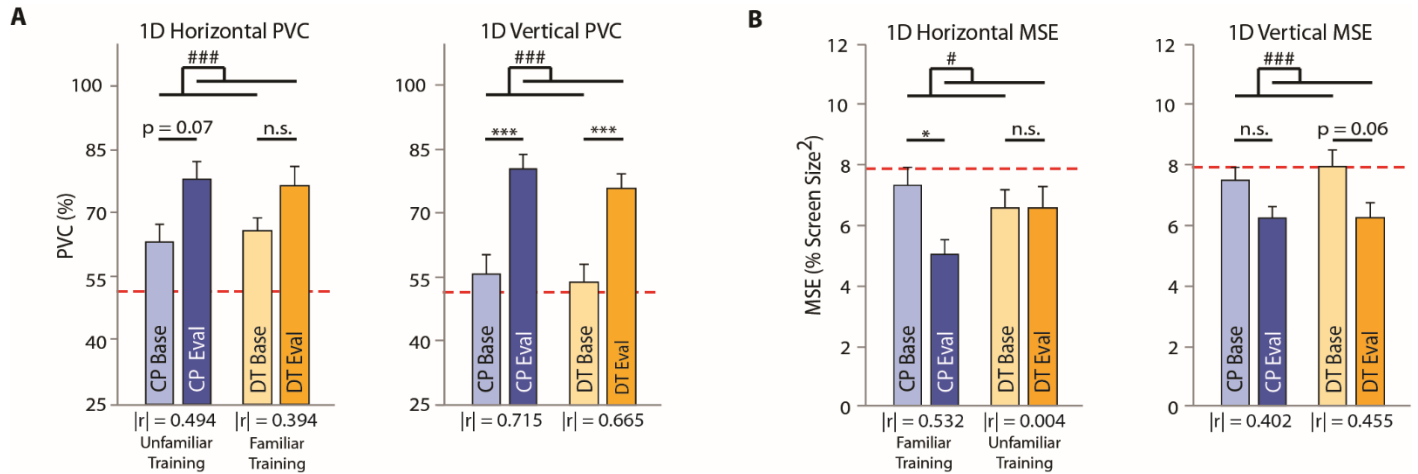


Figure S3. Continuous Pursuit vs. Discrete Trial BCI Learning. (A) 1-dimensional (1D) horizontal and vertical performance values for the DT task at baseline and evaluation for the CP and DT training groups. (B) 1D horizontal and vertical performance values for the CP task at baseline and evaluation for the CP and DT training groups. The red dotted line indicates chance level. Bars indicate mean + standard error of the mean (SEM). The effect size, $|r|$, is indicated under each pair of bars. Statistical analysis using a repeated measures two-way ANOVA ($n=11$ per group) with main effects of time ($\# p < 0.05$, $### p < 0.005$) and training task. Tukey's HSD post hoc test: $* p < 0.05$, $*** p < 0.005$.

Fig. S4.

Supplementary figure 4 displays the group-level spatial and spectral characteristics of the vertical (a) and horizontal (b) eye movement EEG independent components (ICs). The timeseries of these ICs were utilized to determine if the user's gaze played a role in driving cursor movement (Fig. 2g). While eye activity in general was loosely correlated with cursor movement for both vertical and horizontal dimensions, ($R^2 < 0.1$), it was significantly lower during the CP task compared to the DT task.

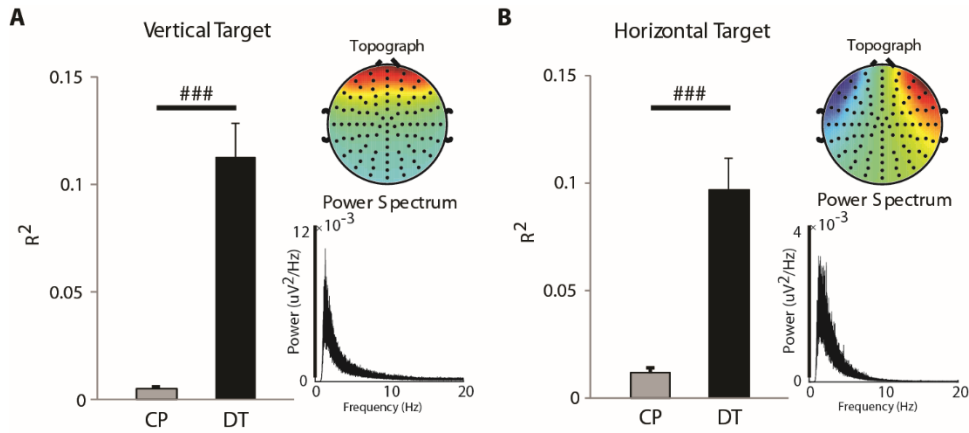


Figure S4. Influence of Eye Activity on BCI control. A-B: Regression output between the vertical (A) and horizontal (B) eye activity EEG independent component activation timeseries and target position. The EEG topography and power spectrum of the corresponding IC are displayed to the right. Bars indicate mean + SEM. Statistical analysis using a repeated measures two-way ANOVA ($n=11$ per group) with main effects of time and task (### $p < 0.005$).

Fig. S5.

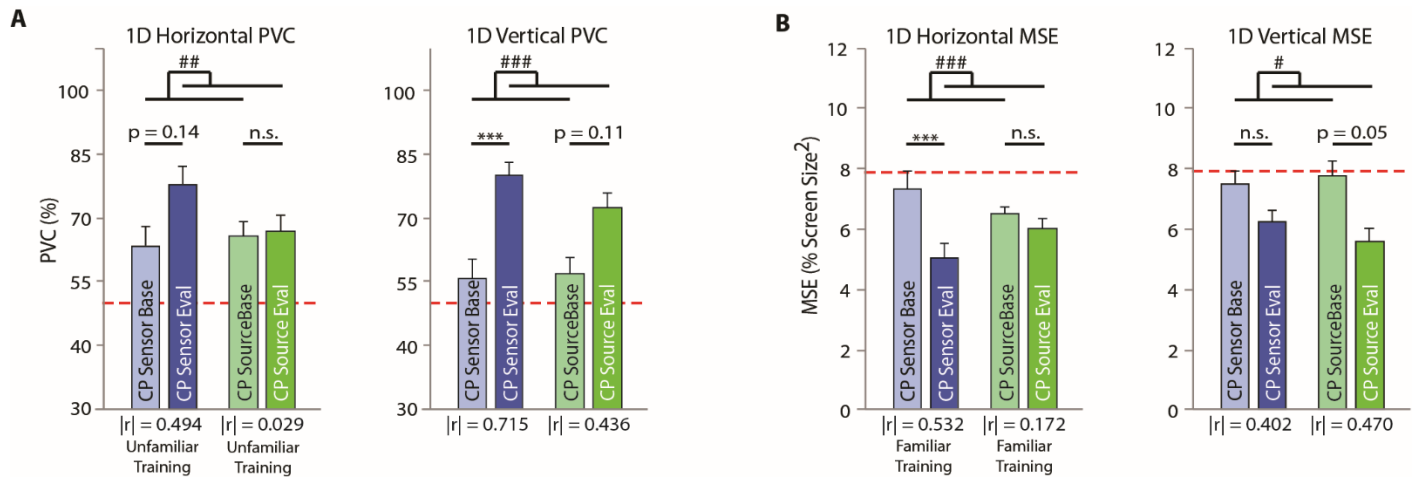


Figure S5. Source vs. Sensor BCI Learning. (A) 1-dimensional (1D) horizontal and vertical performance values for the DT task at baseline and evaluation for the CP (sensor) and sCP (source) training groups. (B) 1D horizontal and vertical performance values for the CP task at baseline and evaluation for the CP (sensor) and sCP (source) training groups. The red dotted line indicates chance level. Bars indicate mean + SEM. The effect size, $|r|$, is indicated under each pair of bars. Statistical analysis using a repeated measures two-way ANOVA ($n=11$ per group) with main effects of time ($\# p < 0.05$, $\#\# p < 0.01$, $\#\#\# p < 0.005$) and training neurofeedback domain. Tukey's HSD post hoc test: $* p < 0.05$, $*** p < 0.005$.

Fig. S6.

Supplementary Figure 6 highlights the procedure for deriving the spatial extent threshold for statistical testing from the squared error histograms. Gamma functions were fit to the histograms and the effect size at each bin was calculated. The extent at which the effect size changed from positive to negative was used as the spatial threshold.

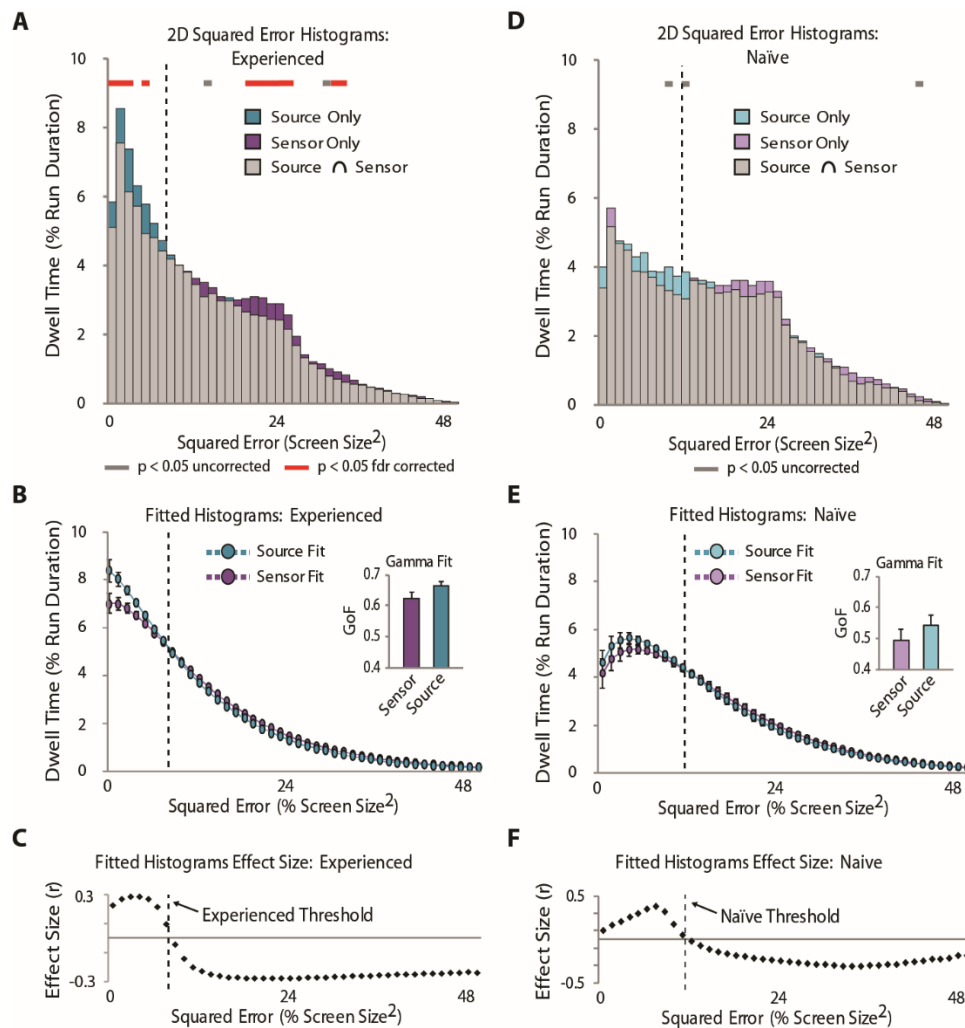


Figure S6. 2D CP Source vs. Sensor Spatial Threshold. A-C: Experienced **user** data (n=16). (A) Group-level squared-error histograms for 2D CP sensor and source cursor control (taken from Fig. 5b, d). (B) Group-level histograms fit with a gamma function. Goodness-of-fit values (GoF) are displayed in the inlay to the right. (C) Effect sizes between the source and sensor fitted histogram at each bin. The point at which the effect size change from positive to negative was defined as the extent threshold used for statistical testing. D-F: Naïve **user** data (n=13), same as A-C.

Fig. S7.

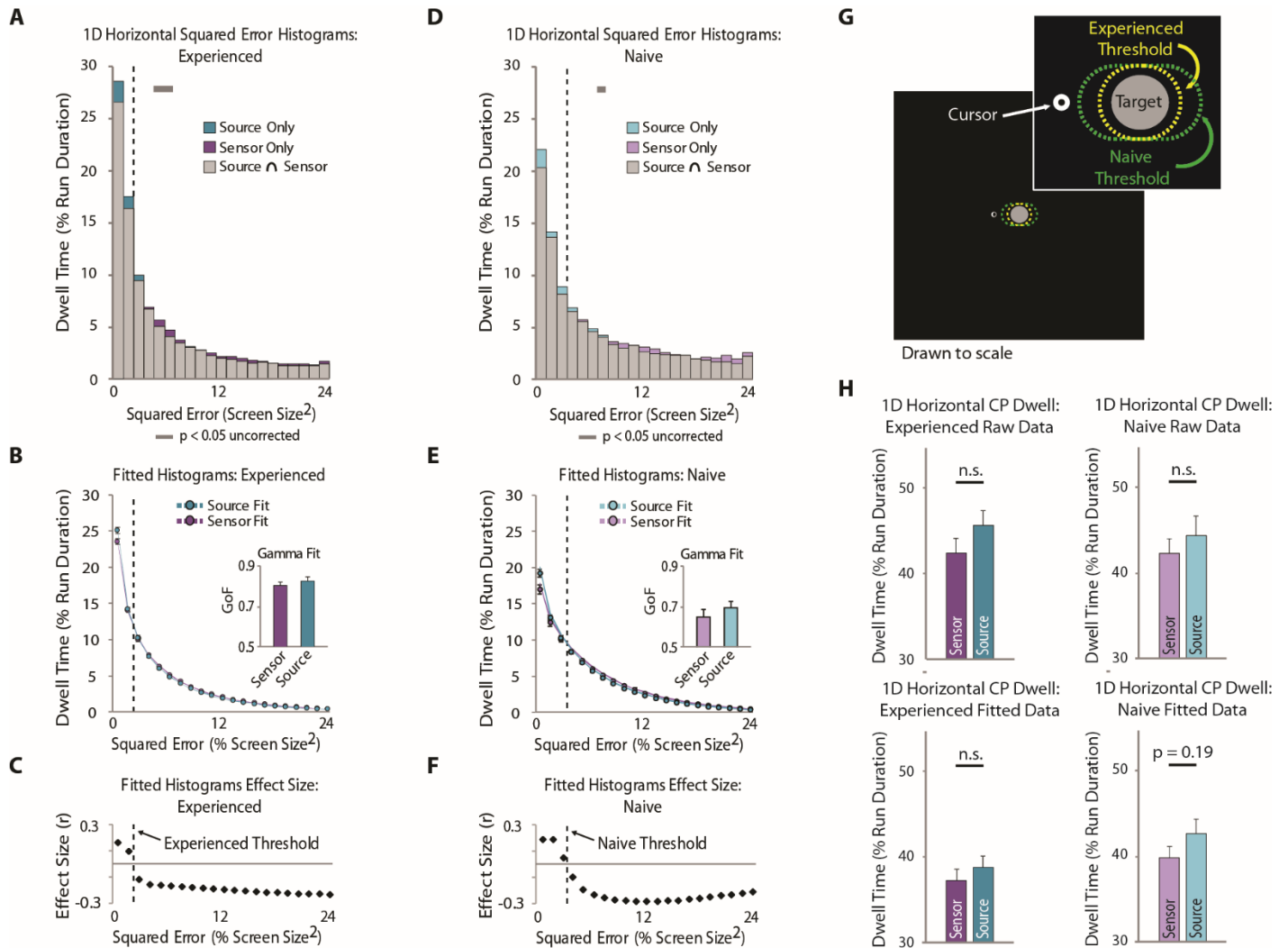


Figure S7. Online 1D Horizontal CP Source vs. Sensor BCI Performance. A-C: Experienced user data ($n=16$). (A) Group-level squared-error histograms for 1D horizontal CP sensor and source cursor control. (B) Group-level histograms fit with a gamma function. Goodness-of-fit values (GoF) are displayed in the inlay to the right. (C) Effect sizes between the source and sensor fitted histograms at each bin. D-F: Naive user data ($n=13$), same as A-C. (G) Scale drawing of the continuous paradigm workspace displaying the spatial threshold derived from for experienced (yellow) and naive (green) users derived from the fitted histogram effect size plots in C and F. (H) Cursor dwell time within the spatial threshold for experienced (left) and naive (right) users using the raw (top) and fitted (bottom) histogram data. Bars and circles indicate mean \pm SEM. Statistical analysis using a one- (naive) or two-way (experienced) ANOVA with main effects of time, and time and decoding domain, respectively.

Fig. S8.

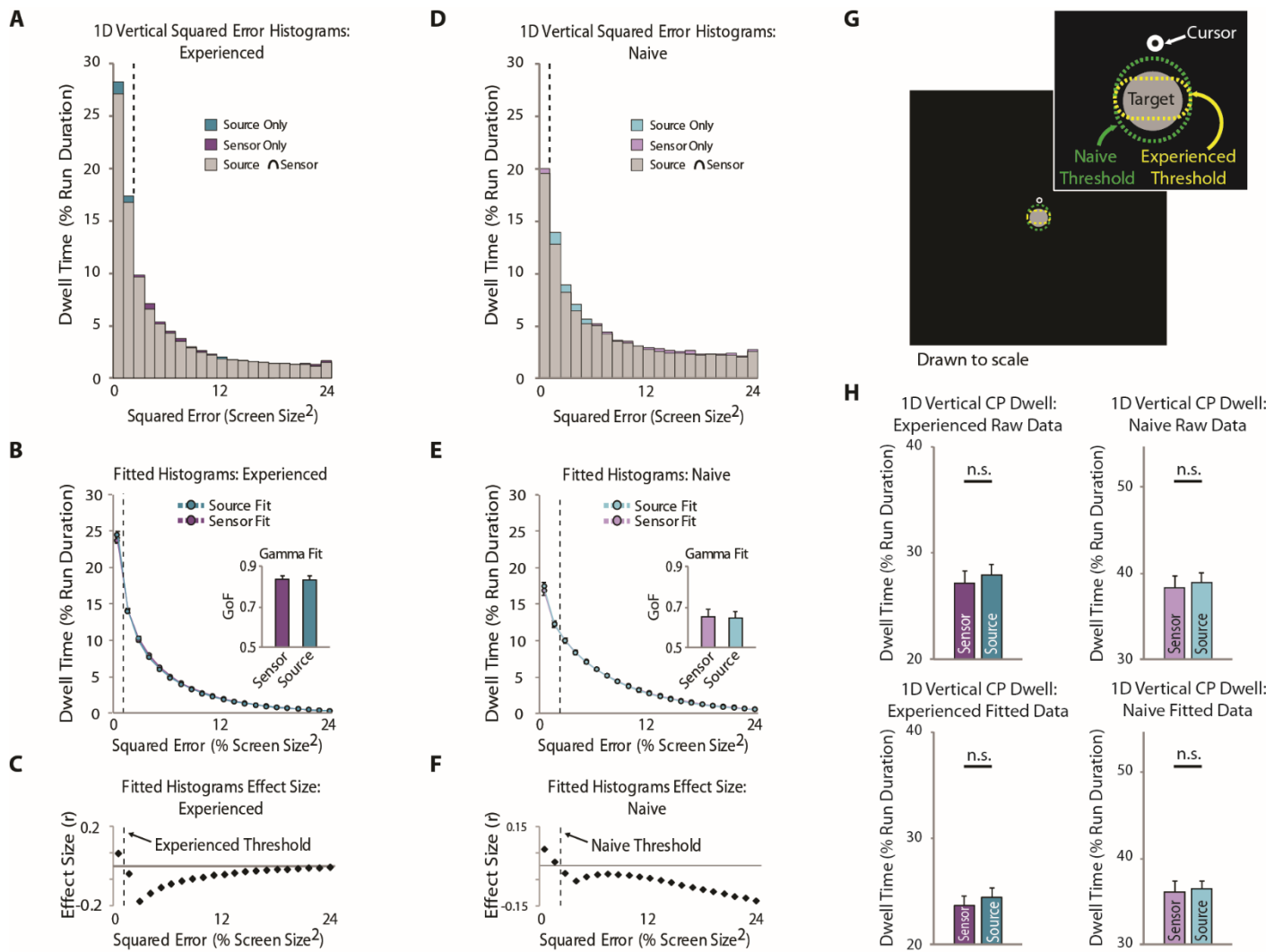


Figure S8. Online 1D Vertical CP Source vs. Sensor BCI Performance. A-C: Experienced **user** data (n=16). (A) Group-level squared-error histograms for 1D vertical CP sensor and source cursor control. (B) Group-level histograms fit with a gamma function. Goodness-of-fit values (GoF) are displayed in the inlay to the right. (C) Effect sizes between the source and sensor fitted histograms at each bin. D-F: Naïve **user** data (n=13), same as A-C. (G) Scale drawing of the continuous paradigm workspace displaying the spatial threshold derived for experienced (yellow) and naive (green) users derived from the fitted histogram effect size plots in C and F. (H) Cursor dwell time within the spatial threshold for experienced (left) and naive (right) users using the raw (top) and fitted (bottom) histogram data. Bars and circles indicate mean \pm SEM. Statistical analysis using a one- (naïve) or two-way (experienced) ANOVA with main effects of time, and time and decoding domain, respectively.

Fig. S9.

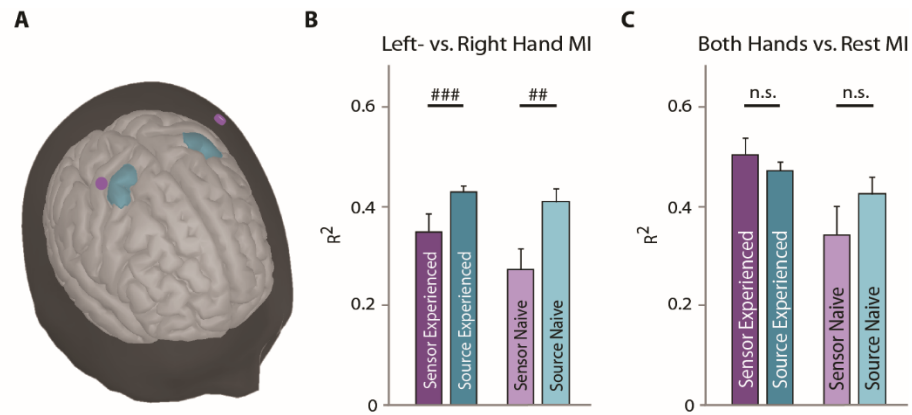


Figure S9. Offline Source vs. Sensor Sensorimotor Modulation. (A) Conceptual illustration of the bilateral sensors (C3/C4) and cortical patches (left/right hand knobs) that are thought to best produce/capture various hand motor imagery task signals. B-C: Maximum R^2 values found in the sensor and source sensorimotor locations identified in (A) for horizontal (B) and vertical (C) commands. Bars indicate mean + SEM. Statistical analysis using a rank-transformed one-way ANOVA with a main effect of decoding domain (n=13 naïve users) and a rank-transformed repeated measures two-way ANOVA with main effects of time and decoding domain (n=16 experienced users). Main effect of decoding domain: ## $p < 0.01$, ### $p < 0.005$.

Table S1.

Supplementary Table 1 highlights the impact of source control on online CP BCI performance in naïve and experienced users. Specifically, we wanted to draw comparisons among online (Fig. S7-8) and offline (Fig. S9) changes between source and sensor control. We observed strong positive effects of source control over sensor control for 1D horizontal control, whereas relatively small effects were observed for 1D vertical control. This is consistent in naïve and experienced **users**. From Fig. S9, we also found a significant improvement in the modulation index for horizontal motor imagery commands when using source features (in both naïve and experienced users) and no significant improvement for vertical commands.

Table S1: Absolute effect sizes for source- vs sensor-based continuous pursuit control

	Absolute Effect Size $ r $		p-value	
	Naïve	Experienced	Naïve	Experienced
1D Horizontal	0.22	0.16	0.21	$1.60 \cdot 10^{-2}$
1D Vertical	0.07	0.05	0.66	0.54
2D	0.28	0.25	0.11	$5.5 \cdot 10^{-3}$

Table S2.

Table S2: Source level sensorimotor region of interest anatomical structures

Structure	Laterality
Paracentral Lobule	Bilateral
Subcentral area (Brodmann area 43)	Bilateral
Postcentral Gyrus	Bilateral
Postcentral Sulcus	Bilateral
Precentral Gyrus	Bilateral
Precentral Sulcus	Bilateral
Central Sulcus	Bilateral
Marginal Sulcus	Bilateral

Videos S1-S3.

Videos S1-S3 display videos of reconstructed real-time, closed-loop virtual cursor control in the unconstrained (original) CP task. The target is the large gray circle and the user-controlled cursor is the small black and white circle. The white border indicates the edges of the workspace. The top two plots on the right display the x and y positions of the cursor (solid colored lines) and target (white dotted line). These positions are normalized to the screen size and carry values between 0 and 1. The bottom plot on the right indicates the total squared error, measured as the square root of the normalized Euclidean distance between the target and cursor. All trials last 60 seconds. Videos are shown at 1.5x speed.

Video S1. 1D horizontal continuous pursuit (unconstrained) BCI virtual cursor control example trial

Video S2. 1D vertical continuous pursuit (unconstrained) BCI virtual cursor control example trial

Video S3. 2D continuous pursuit (unconstrained) BCI virtual cursor control example trial

Videos S4-S7.

Videos S4-S7 display live videos of real-time, closed-loop robotic arm (videos S4-S6) or virtual cursor (video S7) control in the physically constrained CP task. The target is the large gray circle and the user-controlled robotic arm (videos S4-S6) is out of the plane of the computer screen. In video S7, the user controlled the small black and white cursor as in videos S1-S3. The top two plots on the right display the x and y positions of the cursor (solid colored lines) and target (white dotted line). These positions are normalized to the screen size and carry values between 0 and 1. The bottom plot on the right indicates the total squared error, measured as the square root of the normalized Euclidean distance between the target and cursor. All trials last 60 seconds. Videos are shown at 1.5x speed.

Video S4. 1D horizontal continuous pursuit (physically constrained) BCI robotic arm control example trial

Video S5. 1D vertical continuous pursuit (physically constrained) BCI robotic arm control example trial

Video S6. 2D continuous pursuit (physically constrained) BCI robotic arm control example trial

Video S7. 2D continuous pursuit (physically constrained) BCI virtual cursor control example trial